

Preliminary analysis of alternative divertors for DEMO

F. Militello^{a,*}, L. Aho-Mantila^b, R. Ambrosino^c, T. Body^d, H. Bufferand^e, G. Calabro^f, G. Ciraolo^e, D. Coster^d, G. Di Gironimo^c, P. Fanelli^f, N. Fedorczak^e, A. Herrmann^d, P. Innocente^g, R. Kembleton^h, J. Lilburne^a, T. Lunt^d, D. Marzullo^c, S. Merriman^a, D. Moulton^a, A.H. Nielsenⁱ, J. Omotani^a, G. Ramogida^j, H. Reimerdes^k, M. Reinhart^h, P. Ricci^k, F. Riva^a, A. Stegmeir^d, F. Subba^l, W. Suttrop^d, P. Tamain^e, M. Teschke^d, A. Thrysoeⁱ, W. Treutterer^d, S. Varoutis^m, M. Wensing^k, A. Wilde^a, M. Wischmeier^d, L.Y. Xiang^a

^a UKAEA, Culham Science Centre, Abingdon, Oxon, OX14 3DB, UK

^b VTT Technical Research Centre of Finland, FI-02044 VTT, Finland

^c C.R.E.A.T.E. Consortium, ENEA, Napoli, Italy

^d Max-Planck Institut für Plasmaphysik, D-85748 Garching, Germany

^e CEA, IRFM, 13108 St. Paul-Lez-Durance, France

^f DEIm Department, University of Tuscia, Largo dell'Università, 01100 Viterbo, Italy

^g Consorzio RFX, Euratom-ENEA Association, C.so Stati Uniti 4, I-35126, Padova, Italy

^h Eurofusion PMU, Boltzmannstrasse 2, D-85748 Garching, Germany

ⁱ PPF, Department of Physics, DTU, DK-2800 Kgs. Lyngby, Denmark

^j ENEA, Via Enrico Fermi 45, I00044, Frascati (RM), Italy

^k Swiss Plasma Center (SPC-EPFL), CH-1015 Lausanne, Switzerland

^l NEMO Group, Politecnico di Torino, Corso Duca degli Abruzzi 24, 10129, Torino, Italy

^m Karlsruhe Institute of Technology (KIT), Karlsruhe, Germany

ARTICLE INFO

Keywords:

Alternative divertor configurations

Divertor design

DEMO

ABSTRACT

A physics and engineering analysis of alternative divertor configurations is carried out by examining benefits and problems by comparing the baseline single null solution with a Snowflake, an X- and a Super-X divertor. It is observed that alternative configurations can provide margin and resilience against large power fluctuations, but their engineering has intrinsic difficulties, especially in the balance between structural solidity and accessibility of the components and when the specific poloidal field coil positioning poses further constraints. A hybrid between the X- and Super-X divertor is proposed as a possible solution to the integration challenge.

1. Introduction and methodology

As fusion enters the delivery era, and the community plans and designs large machines in the reactor class, a greater emphasis is placed on the issues associated with the exhaust of the plasma. These include, but are not limited to, the protection of the surfaces of all the components exposed to the plasma, both in steady state and during transients, the efficient pumping of the helium ashes, which would otherwise choke the fusion reactions, the minimization of the pollution of the core plasma from intrinsic and seeded impurities. While all these essential functions of an exhaust system must be ensured in a reactor, the biggest challenge is to integrate them among each other and especially with the rest of the machine. Indeed, it is crucial that the performance of core physics is not degraded by the exhaust design

choices and, equally, that these are compatible with the often severe engineering constraints that a reactor will have.

The problem is exacerbated by the fact that next generation devices will be much more demanding than current machines in terms of both physics and engineering. The power that needs to be handled by the exhaust system scales with the fusion power we want to achieve, and this fact is in the most fundamental laws of fusion physics, as it is connected with the production of α particles. Practically, this means that for a \sim GW reactor the power that needs to be safely absorbed by the walls is in the hundreds of megawatts, at least one order of magnitude larger than what we are experiencing in today's largest tokamaks. Additionally, neutron irradiation with unprecedented high fluence, very large confining fields (\sim 10 T) and plasma currents (\sim 15 MA), contributes to the challenge. Finally, the engineering of the

* Corresponding author.

E-mail address: fulvio.militello@ukaea.uk (F. Militello).

<https://doi.org/10.1016/j.nme.2021.100908>

Received 31 July 2020; Received in revised form 22 December 2020; Accepted 6 January 2021

Available online 13 January 2021

2352-1791/Crown Copyright © 2021 Published by Elsevier Ltd.

This is an open access article under the CC BY-NC-ND license

(<http://creativecommons.org/licenses/by-nc-nd/4.0/>).

reactor poses new limitations on what can be built, as plasma facing material properties, remote maintenance and installation, port dimensioning and acceptable forces and stresses on the structural components all conspire to complicate the design.

Focusing on the exhaust system, one of the biggest concerns is to find an operational space that is sufficiently robust and reliable, even in the presence of unavoidable off-normal events and under uncertainty. In particular, the first line of defence against the exhausted power, the divertor, has to be able to sustain steady state loads that, if unmitigated, would reach hundreds of MW/m², well beyond acceptable structural limits for the plasma facing components. Additionally, once in the operating mitigated state, the divertor needs to be able to dissipate the additional power that unexpected transients could produce (maybe from failed pellet injection, radiation fluctuations or emergency ramp downs).

The European DEMO design [1] is based on the ITER exhaust solution: a single null divertor (SND) with vertical targets [2,3]. However, extrapolation is not obvious, as the two machine will operate in different regimes. Core radiation will be much larger in DEMO (~66% versus ~33% in ITER) but with similar power crossing the separatrix (~150 MW for DEMO and ~100 MW for ITER). This means that DEMO will have a large upstream reservoir of power (~300 MW versus ~50 MW) that can endanger a divertor fully detached and under a lot of strain. To give the measure of the problem, a 10% variation in core radiation would unleash an additional ~30 MW towards a divertor that in its ideal operation point already needs to dissipate 90% of the power it receives (optimistically assuming a wetted area of 3 m² and material limits at 5 MW/m²). The DEMO divertor will therefore need to operate in fully detached conditions (ITER will be semi-detached), which implies that there is a risk the detachment front could reach the X-point and cool off the pedestal or destabilize the discharge. Active detachment control, however, might not be possible in DEMO due to lack of neutron resistant sensors and actuators, thus solutions that provide passive stabilization of the detachment front would be helpful.

These observations motivate research of alternative divertor configurations (ADCs) for the plasma exhaust. EUROfusion has studied these alternatives in a systematic way and initial results were already reported elsewhere [4]. Here we give an updated and comprehensive report of recent and important finding in this area, which mix both physics and engineering considerations. While the potential benefits need to be weighted against the unavoidable cost that the additional complexity entails, the latter must be accepted if the SND cannot provide a solution. In particular, we investigated four ADCs: the double null (DNND), the Snowflake (SFD) [5,6], the X (XD) [7] and Super-X (SXD) [8] divertors. Apart from the first, which will be treated in a separate publication [9], each other one will be discussed independently and from their comparisons we will draw our conclusions.

It is in the nature of our analysis to be comparative. Indeed, given the large uncertainties on exhaust physics and technology, and the unprecedented level of complexity of the problem, the only wise approach is to dismiss predictions that aim at absolute values and rather focus on similarities, differences and trends observed between the configurations investigated. This, however, requires a rigorous methodology in which analyses are carried out in a standardized way, with the same tools and with agreed procedures, so that the comparison is fair. Despite the triviality of this argument, its practical application is far from easy.

The second important methodological aspect is that the work presented was deeply integrated, with cross-fertilization and continuous exchanges between the physics and engineering aspects, so to form a consistent picture where each configuration analysed can be represented as a single entity. This is the way we choose to present our results, with one section for each solution, despite the fact that the actual work was carried out across configurations.

Finally, the results presented here must be interpreted as a step in the right direction rather than a conclusive assessment of the properties of the ADCs, or a recommendation for how to build an exhaust system

for a reactor. Indeed, we started from ADCs for DEMO that included the features that were originally predicted to be beneficial, but that are not yet optimized. This initial attempt cannot lead to the 'right' solution straight away, as this must be the result of iterations based on the lessons learned.

2. Configurations and reference

Our analysis started with equilibria previously elaborated and discussed in [4], see Fig. 4 in that paper. For each configuration, it is possible to find a solution that is sustained only by external coils (i.e. external to the toroidal coils cage) and in which forces and macroscopic engineering constraints are satisfied (see [4] for further details, including the machine characteristics). More refined structural calculation, which show issues for the mechanical stresses in the toroidal field coils, will be discussed later on. While the analysis on this paper will be based on the '2018' configurations discussed in [4], new and updated 2D poloidal sections have been further elaborated and modified to include ports compatible with remote handling and are shown in Fig. 1, where also the vacuum vessel (VV), the breeding blankets (BB), the toroidal (TF) and poloidal (PF) coils are depicted. The position of the PF coils and the shape of the TF coils is optimized as far as the constraints discussed above are concerned. However, the configurations are not yet designed to achieve optimal structural conditions in the TF coils or for the maximization of the physical benefits.

The SND design is the baseline DEMO divertor and will be used as a reference against all the other designs. This configuration is more optimized on the engineering side, and already incorporates refined considerations on divertor, remote handling [1] and breeding blanket integration. We therefore had to simplify some of its features so that it could be at the same level of maturity of the ADCs in order to have a fair comparison (especially for structural calculations).

Multifluid simulations were carried out with SOLPS-ITER in order to identify the operating space of the machine, defined as the parameter set when the maximum heat flux on the divertor is below 10 MW/m², the target temperature is below 5 eV (due to limits on the erosion), and the separatrix Greenwald fraction is below 0.6. The simulations evolved Deuterium, Helium and Argon (used as a seeded impurity and bunched), assumed fluid neutrals, no drifts and a fusion power of 2GW. This implies that, with a core radiation fraction of 66%, the power crossing the separatrix accounts for 150 MW. Also, given the fusion power, also the core Helium production rate is fixed at $7 \cdot 10^{20}$ particles per second. A core Deuterium puffing rate of $3.5 \cdot 10^{22}$ particles per second simulates pellet injection, while gas puff is used as a scanning parameter, Γ_D , as well as the Ar seeding rate, Γ_{Ar} . All equilibria had the same target angle of 1.5° to ensure a fair comparison. Large uncertainties afflict the predictions of the transport coefficients, which are therefore fixed by rescaling the values used for ITER simulations [3] in such a way that the midplane heat flux decay length is 3 mm. Therefore, $D = 0.1$ m²/s and $\chi_i = \chi_e = 0.3$ m²/s in the SOL, with the heat transport coefficients reduced to 0.17 m²/s in the transition region spanning 5 mm inside the separatrix and to 0.1 m²/s in the core (i.e. deeper than 5 mm from the separatrix). This roughly simulates a temperature pedestal with a weaker density pedestal, representative of generic no-ELM regimes. We recognize that, while imposing identical diffusion coefficients for all the configurations provides a fair comparison, it also implies that our simulations can assess only the geometrical benefits of the ADCs and not their potential gain in terms of perpendicular transport. The use of configuration dependent poloidal distributions and amplitudes of D and χ will be a goal for the future and should be guided by turbulent analyses. The fluid approximation for the neutrals should be revised in future work as it neglects fast neutral populations and their interaction with the machine geometry as well as molecular effects. It is partially justified, however, by the fact that in the operating regime the neutral mean free path in the whole divertor, including the private flux region, is less than 5 cm (typical densities and temperatures are of the order

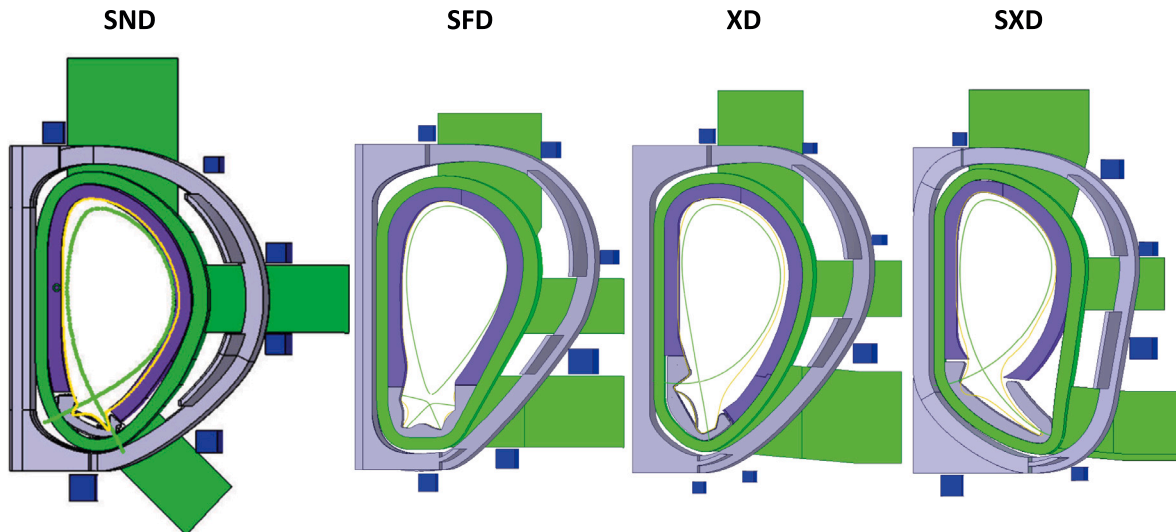


Fig. 1. Cross sections for the different configurations. TF coils and intercoil structures and divertor cassette in grey, PF coils in blue, BB in purple, VV and ports in green. The plots are not in scale, as the plasma volume is constant in all cases (2350 m^3). (For interpretation of the references to colour in this figure legend, the reader is referred to the web version of this article.)

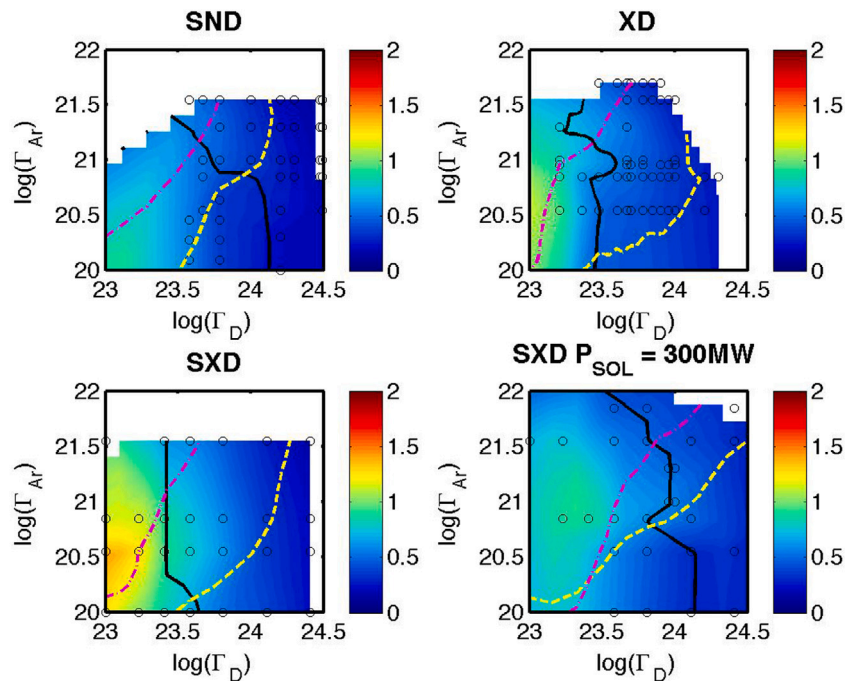


Fig. 2. Comparison between operating spaces in different configurations. The colour plot represents the He concentration at the outer midplane separatrix (in %) as a function of the base 10 logarithm of the imposed Deuterium, Γ_D and Argon Γ_{Ar} fluxes, measured in s^{-1} . The lines are isocontours of the maximum temperature on the entire (inner and outer) divertor surface (solid), Greenwald fraction at the separatrix (dashed) and Ar concentration at the outer midplane separatrix (dot-dashed). They represent the threshold of $T_{max} = 5 \text{ eV}$, $f_{GW} = 0.6$ and $c_{Ar} = 1\%$, respectively. The constraint on the target heat load is not shown because it is always less stringent than the temperature one. (For interpretation of the references to colour in this figure legend, the reader is referred to the web version of this article.)

of 10^{18} – 10^{20} m^{-3} and 2–3 eV), while the size of the smaller divertor we examined is larger than 2 m. The in/out divertor asymmetry might be affected by fluid drifts, which were turned off in our simulations. However, we can speculate that similarly to ITER results [10] drift effects will become more marginal at larger collisionality, which is the regime we care about, and that they will induce more loads on the outer target, which is typically more protected in the alternative configurations. Additional information on the multifluid simulation set-up can be found in [9,11,12]. The results of the simulations for the reference case are shown in Fig. 2, where He concentration at the separatrix density is plotted as a function of the seeding and fuelling

levels. Additional curves bound the acceptable operating regime, as given by the physics constraints discussed in the previous paragraph plus the separatrix Ar concentration. The acceptable operating space lies in the region internal to these curves. A potential concern, is the Tritium throughput in a 50%–50% mix, which is very large for all the configurations (~ 3 – 5 kg/h). However, our performance could be maintained by decreasing the throughput and reducing the pumping efficiency, as done for the ITER simulations [3].

Simulations carried out with state-of-the-art European 3D SOL turbulence codes (GBS, GRILLIX, STORM/BOUT++, TOKAM3X) show filamentary transport in the Scrape Off layer both above and below the

X-point, confirming experimental observations and previous numerical results. These 3D simulations are too computationally intensive for realistic DEMO parameters and hence they had to be rescaled to medium size tokamak dimensions. While this will surely affect the physics, it should still allow comparison between different designs and especially provide a first indication of the poloidal variations of the transport coefficients.

Moving to engineering, Finite Element Method structural calculations of the TF coils were performed using ANSYS, focusing on the effect of the electromagnetic (EM) loads. These can be divided into hoop forces, describing the expansion of a closed current carrying conductor, and out-of-plane forces, generated by the interaction between the TF coil current and the poloidal magnetic field induced by the PF coils. The hoop forces can be minimized by producing a constant tension design known as Princeton D-shape [13]. Clearly, the ADCs cannot be designed with this optimal bending-free solution in mind, and we will see that this creates issues. However, also the current version of the SND design is not optimized in this respect and the shape of the TF coils will probably need to be modified to be capable to withstand the EM forces. This will either require the increase of their height or their number. In terms of limits, stress linearization was used to assess the designs where the peak static stress intensity appears to be problematic [14]. The allowable stress value, S_m , is set to 2/3 of the material's yield strength at a temperature of 4 K, which is 1000 MPa for the EC1 strengthened austenitic steel we consider. According to the RCC-MRx rules, the primary membrane stress, P_m , must be such that $P_m < \alpha S_m$, the primary membrane plus bending stress, P_{mb} , such that $P_{mb} < 1.3\alpha S_m$ and the primary membrane plus bending plus peak stress P_{mbp} , such that $P_{mbp} < 1.5\alpha S_m$. High and low field side parts of the TF coil have different limits, so that for the former $\alpha = 1$ and for the latter $\alpha = 3/4$, reflecting the fact that the inner section is forged and the outer cast.

The analysis was performed using a simplified winding pack geometry composed by six layers with smeared material properties meshed with hexahedral elements, while the case and the filler use tetrahedral elements to improve the contact behaviour (a friction coefficient of 0.3 has been chosen between the casing and the filler, which can slide). The boundary conditions simulate the periodic behaviour between individual TF elements. In reality, the inner leg of the TF coils can slide with respect to each other and we carried out a series of stress analyses allowing for the possibility of separation. However, our preliminary results show that the differences between the two approaches are small as far as equivalent stresses are concerned, thus giving us confidence in our simplified approach. Finally, the stress state is converged with respect to mesh refinements.

For the sake of comparison, we have simplified the refined SND DEMO engineering design to the level of our ADC configurations. With this in mind, our structural calculations, show stresses against cooldown (from ambient temperature to 4 K) and EM forces several tens of percent above threshold at the connection between inner and outer limb of the lower part of the TF coil (see Fig. 3). While this number is given to compare with our current ADCs designs, these stresses are likely to be significantly reduced by more detailed engineering, and thus are not cause for concern.

In addition to the integrity of the structures surrounding the plasma, we have also examined the response of the equilibrium to perturbations representing unwanted, but sometimes unavoidable, changes in pressure or current profiles. In particular, we have assumed fluctuations during the flat top phase that change by roughly 10% the plasma induction, I_i , and in the ratio between kinetic and poloidal magnetic pressure, β_p . In our baseline case, $I_p = 19$ MA, $I_i = 0.8$ and $\beta_p = 1.14$. In addition, the growth rate of the vertical instability was assessed at flat top and at the start of ramp down, when conditions are more challenging due to the fact that the current is peaked and β_{pol} is low. The SND configuration, which has already been optimized, does not cause concerns, as the growth rates are $\gamma_{FT} \approx 2.3$ s⁻¹, $\gamma_{SRD} \approx$

6.3 s⁻¹ and the vertical displacement once the plasma equilibrium is perturbed induce a vertical displacement of around 2 cm, well within safety limits. Another important parameter to assess is the capability of the system to recover from a vertical displacement event of a certain magnitude in terms of the power required by the stabilizing coils. A 5 cm displacement in SND can be stabilized with only ex-vessel coils with less than 350 MW in all the regimes considered.

Finally, all configurations have been analysed to assess their accessibility for remote maintenance and component installation. The SND has been extensively analysed in this respect and information on its challenges and solutions can be found in [1].

3. Snowflake divertor

The potential advantages of the SFD configuration are threefold, one is to distribute the power and particle fluxes on multiple legs, the second is to provide an increase of the connection length at its hexapole null and the third is to allow a stable radiation region between the two nulls and hence outside the main plasma.

Obtaining SOLPS results for this configuration is challenging, as only recently the code has acquired the capability to perform SFD simulations [15]. The magnetic equilibrium we examined is a SFD — (secondary X-point in the low field side SOL) with a gap between the separatrices at the midplane of 1 mm. Unfortunately, the simulations converged only in a region of the parameter space with low Ar and D levels and are hence not shown (one order of magnitude lower than the SND). Comparing the data with the SND, it is thus no surprise that one of the divertor legs (the outermost) is still in attached regime and is exposed to very large heat fluxes and target temperatures. Due to these technical difficulties, it is therefore not yet possible to reliably assess the potential benefits of this configuration. Efforts are ongoing to examine 4 mm, 10 mm and 40 mm gaps, but the results of this work are not yet mature and will be presented in a dedicated follow up paper.

On the other hand, some conceptual progress was achieved on the basic mechanisms underlying the physics of the SFD. In particular, 3D turbulent simulations were performed with the GBS code [16], albeit for analytic equilibria and plasma parameters much more forgiving than DEMO's. What was observed was that a convective cell forms in the proximity of the X-point, which contributes to redistribute the plasma among the four strike points. The mechanism associated with the convective cell is novel and does not appear to be the electromagnetic churning mode described in [17], as the simulations discussed here are electrostatic. More details on these simulations and their results can be found in [16] and some connected investigation in SND geometry in [18].

In terms of the structural calculations of the TF coils, we have identified two issues where inner and outer segments meet and at the connection between the intercoil structures and the casing just below the equatorial port. In both cases, the stresses exceed one of the thresholds, but these conditions were less severe than for the SND, with the equatorial port failing only by a couple of percent, see Fig. 3. These peaks appear at sharp corners, which could be smoothed with fillets in more refined designs, and thus only cause moderate concern.

On the other hand, the current design is probably underestimating the stresses in the TF coil, since the intercoil structures used have an unacceptable poloidal extension. Indeed, a major issue for the SFD is the accessibility of the divertor region for installation and remote handling operations. A remote maintenance assessment carried out *a posteriori* showed that the calculations presented here are not yet compatible with the divertor cassette removal as the intercoil structures encroach into the lower port and the inner blanket removal would not be possible. This has the unfortunate consequence that the structure's rigidity will be lowered in future designs due to the removal of the excess material. In general, a fundamental complexity and weakness of the SFD is the need to bring PF5 and PF6 close to the bottom low field side part of the TF coil while remaining sufficiently separated to

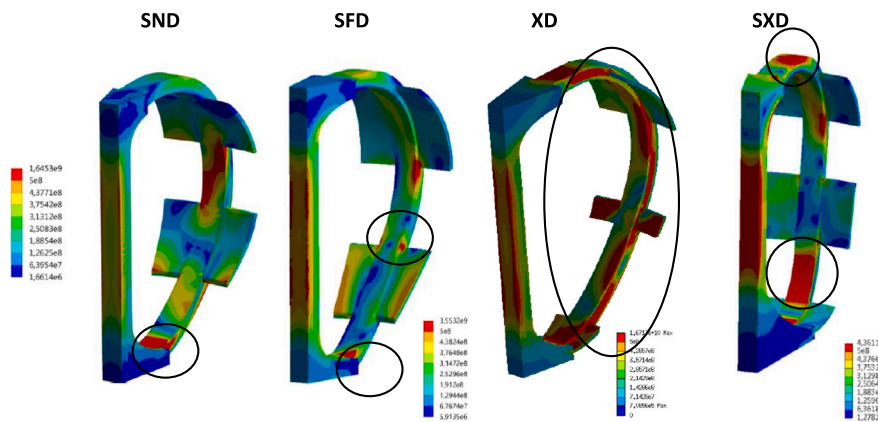


Fig. 3. Stress map for the different configurations (in Pa). Note that the maximum of the colourmap is based on the outer limb peak threshold of 500 MPa, which is the most conservative limit. Hence several areas present acceptable stresses despite being red. The black ellipses identify areas where stresses are unacceptably high. (For interpretation of the references to colour in this figure legend, the reader is referred to the web version of this article.)

efficiently generate the hexapole null (here we count PF coils clockwise starting from the top). This creates problems of space for the lower port and therefore of accessibility of the divertor.

Another worrying and intrinsic feature of the SFD is its susceptibility to perturbations. While its vertical stability is acceptable, with $\gamma_{FT} \approx 1.73 \text{ s}^{-1}$ and $\gamma_{SRD} \approx 5.36 \text{ s}^{-1}$, the position of its magnetic axis shows displacements of up to 30 cm when l_i or β_{pol} are changed. Furthermore, it is concerning that the shape variations of the separatrix bring the plasma closer to the wall and that the strike point positions have large excursions that could take them outside of the armoured region. Power requirements for the ex-vessel control system appear to be unmanageable in our current designs, with more than 100 MW required to stabilize a 5 cm vertical displacement during the flattop and above 1GW in the ramp down phase.

4. X-divertor

The X-divertor is associated with a large poloidal flux expansion in the vicinity of the target and a consequent increase of connection length and particle residence time in the divertor. Also, the fanning of the flux surfaces close to the plate is considered to be useful to stabilize the motion of the detachment front towards the X-point.

We find that this configuration has indeed beneficial effects in terms of allowing a much wider operational space than the SND in terms of seeding and fuelling levels (see Fig. 2). It is interesting to observe that, differently from the SND, the XD enters the acceptable operating space by increasing the deuterium flux, which seems to be sufficient to induce detached conditions. The role of the Ar impurities is to keep the separatrix density low by absorbing the power that would otherwise go into deuterium ionization and by doing that providing additional radiation.

The preliminary structural calculations for this configuration, however, were performed considering a minimal poloidal extension for outer intercoil structures. The results suggest that a significant redesign is needed, as at the moment they show several difficulties. As shown in Fig. 3, stresses in the outer limb of the TF coils exceed thresholds systematically, and can sometimes be significantly above acceptable limits. This is largely due to the fact that port size was maximized in this configuration, leading to relatively short intercoil structures and a lack of support and rigidity (see also Section 6). While the equatorial and lower port could be reduced to increase the strength of this design, the upper port cannot be further shrunk because it already presents challenges in terms of safe extraction of the inner blanket structures, which would require complex kinematics. In addition to the fact that the upper port should not be enlarged to avoid weakening of the structure, there is no physical space due to the proximity of PF1 and

PF2, so that blanket handling is difficult. These, however, seem to be issues connected with the current design rather than intrinsic to the XD configuration.

Finally, in terms of controllability, the XD shows growth rates comparable to the SND's ($\gamma_{FT} \approx 1.66 \text{ s}^{-1}$, $\gamma_{SRD} \approx 6.73 \text{ s}^{-1}$) but larger vertical displacement in the case of equilibrium modifications (between 10 cm and 15 cm for our usual variations of l_i and β_{pol}). The power required for the vertical stabilization is roughly twice as large than for the SND, thus implying that the start of ramp down phase cannot be handled even for a 5 cm shift. Similarly to the SFD, the strike points of the XD display a significant sweeping during variations of the equilibrium (25 cm for the inner leg and 40 cm for the outer), although they remain on the target plate, thus implying acceptable conditions. The shape of the plasma under perturbations remains significant and larger than the SND's, although less concerning than the SFD and potentially possible to handle.

5. Super-X divertor

The final configuration we discuss is the Super-X divertor, which, according to literature, has a longer outer divertor leg to maximize the toroidal flux expansion (basically, it increases the wetted area by depositing the power on an annulus with larger major radius), increase the connection length, improve neutral trapping and provide passive stabilization of the detachment front as the latter has to move against the magnetic field gradient [19]. We note that our configuration has a marginal outer poloidal flux expansion ($f_x = 2.4$, 30% lower than the SND's), which implies that it should be considered more of a long legged divertor than an archetypal SXD. The reason for this is that generating poloidal and toroidal flux expansion together is extremely difficult when the magnetic equilibrium can be created with only 6 poloidal field coils external to the toroidal field coil cage.

According to the multifluid simulations, similarly to the XD, the SXD has a wider operating space than the SND and detaches thanks to an increase in fuelling levels, see Fig. 2. Most importantly, the SXD has an operating window even with 300 MW crossing the separatrix, corresponding to zero line radiation in the core. This means for a well designed operating point, reattachment should not occur even during the largest power fluctuations that can be achieved in the device. Preliminary analysis, discussed in a companion paper [11,12], suggest that this might be due to the fact that, at the higher power, Ar supplements the required additional radiation as it becomes more efficient at dissipating energy at higher SOL temperatures. The SND cannot achieve that because its operating space at 150 MW already relies on Ar radiation. Although simulations are not mature enough for the XD configuration, we suspect that a mechanism similar to the SXD's might be at play also in that case.

Finally, it is worth remarking that concerns were raised in the past with respect to the asymmetry between in/out power fluxes in the SXD divertor. This is due to simple extended two-point estimates of the power redistribution based on the connection length. The power flows preferentially through the shortest path, leading to a higher load at the outer target in the SND and more balanced load in the SXD (and XD) when the in/out connection lengths are comparable. However, the wetted area at the high field side is smaller, and the energy fluxes are therefore higher, even becoming problematic if the outer connection length becomes excessive. On the other hand, these estimates are based on simplified models that do not include radiation physics and detachment. We find that *both* inner and outer target have acceptable loads and temperatures and the asymmetry is reduced in the SXD and XD in the operating space where the divertor is detached, and hence this does not raise concerns [11,12]. This is compatible with ITER's results at high divertor neutral pressure [3].

We also find that the SXD configuration generates a different pattern of turbulence with respect to the SND. In particular, simulations at a reduced scale show significant turbulent activity in the outer divertor leg, potentially able to increase the perpendicular transport in the divertor region. Also, core filaments shear before reaching the target, thus effectively disconnecting the regions above and below the X-point. While more analysis is required, and especially on the extrapolation to larger devices, these are potentially beneficial effects as far as load spreading is concerned.

While the physics of this configuration seems attractive, it comes with an engineering cost. In particular, the need to extend the outer divertor leg to major radii poses a challenge to coil design, as it implies a significant deviation from the TF D-shape (if one wants to use space efficiently and keep cost contained). Regions of sharp curvature in the lower part of the TF coil are problematic, with stresses just exceeding the threshold by a few percent. In the upper part of the coil, where the inner and outer limb connect, stresses are above the allowed value, but comparable to those found in the SND, see Fig. 3. As this is a preliminary design, we expect that more sophisticated engineering of the TF coil could improve the situation, although care must be taken on the intrinsic difficulties associated with the SXD. In terms of remote maintenance, all ports provide adequate access to both the blankets and the divertor, as long as the divertor cassettes are properly shaped. As a matter of fact, the upper port could be slightly reduced on its high field side to reduce the structural issues discussed above with consequences that can probably be handled on blanket handling extraction.

In terms of plasma control, even in this case vertical stability is comparable to the SND as far as growth rates are concerned ($\gamma_{FT} \approx 2.11 \text{ s}^{-1}$, $\gamma_{SRD} \approx 7.3 \text{ s}^{-1}$). On the other hand the SXD displays shape changes under variations of the equilibrium which are particularly concerning as a they might lead to enhanced interactions with the upper wall. Indeed, while the displacement of the magnetic axis is comparable to the XD, the top of the plasma can shift up to 25 cm upwards. Inner and outer strike points can move up to 40 cm along the targets, but the particular design of the SXD implies that they remain on armoured structures. Power requirements for the ex-vessel vertical control system appear very demanding in the ramp down phase.

6. Discussion

The comparative analysis of the different configurations allows a deeper understanding of the problem of divertor optimization. On the physics, one of the conclusions is that increasing the outer connection length does show an increase in asymmetries, but they become completely irrelevant when the divertor detaches, since both targets remain within acceptable constraints. On the other hand, the outer divertor leg should not be too long and the ratio of the in/out connection length should not be much larger than one to ensure safe power handling in the inner leg and accessible operating spaces (all our configurations satisfy this criterion). Crucially, we found at least

one configuration (SXD) that can allow operations without imposing performance reducing radiation from the core, and we suspect that a second one might lead to similar results. With the caveat that more sophisticated models will have to confirm these results, this means that even in the event of large power transients, the divertor should be able to cope with the additional power flux. In general, it is interesting to see that Ar seeding is less crucial for the ADCs than for the SND, as this could give some extra margin to access higher power conditions. We believe this is due to the fact that a longer connection length reduces the temperatures at the target and increases it upstream, thus creating better conditions for both deuterium and Ar radiation in the two regions and hence an extended operating space (more details are given in [11,12]). Also, Ar injection is efficient at reducing the separatrix density and thus potentially improve performance (this was observed also in ITER simulations [3]). Of course, our multifluid results must be taken with caution as kinetic simulations should confirm these benefits, although we believe the trends identified can provide valuable information, especially in the high fuelling phase of interest (e.g. ITER's simulations are kinetic but show trends similar to ours).

The engineering studies carried out showed that designing ADCs requires a delicate balance between ports and intercoil structures. The latter have to be sufficiently resistant to provide rigidity against out of plane forces and extended to ensure passive stabilization against vertical displacement events. On the other hand, ports have to allow for efficient removal of blanket modules and divertor cassettes, and, in the case of the lower port, give a clear path for pumping purposes. Alternative configurations require PF coils in certain positions to maximize their benefits and this poses additional constraints on the overall design. The bottom part of the machine is the most affected by this issue, although some effects can be seen also in other areas (e.g. the SXD problem near PF1). While certain difficulties can be designed out in more elaborated engineering studies (such as those already carried out for the SND), others are intrinsic to the ADCs and these are the ones that should receive more attention going forward (e.g. the PF coil positioning in the XD and SFD and the TF coil shape for the SXD). Finally, control poses a serious concern, especially for the sensitivity of the plasma shape to current profile variations. In particular, secondary X-points are very susceptible to this and have large excursions in all ADCs, which can be problematic for the configurations that are based on this concept (especially the SFD since its secondary null is in the plasma). The possibility to improve the stability performance of the configurations with appropriate reshaping and with the addition of an in-vessel vertical stabilization system is under analysis.

7. Conclusions and perspectives

The overall analysis of the ADCs presented in this paper has shown a truth that we already suspected: their physics is appealing but their engineering is difficult. However, in many cases we can now identify where improvements are likely, possible or difficult. In particular, it is clear that the challenge of the ADCs is the integration of often conflicting requirements. In this respect, this work would be incomplete without a recommendation on how to optimize an ADC for DEMO.

Based on the physics results obtained, it is clear that large flux expansion (poloidal ad toroidal) and longer outer connection lengths should be sought (especially the latter seemed relevant for our SXD configuration). Extreme solutions, however, clash with engineering constraints, in particular the controllability, the PF coil positioning and the level of stresses in TF coils that diverge from the D-shape. We hence think that a divertor with comparable in/out connection length, outer strike point radius and target poloidal flux expansion as large as possible and good closure (potentially just given by the size of the machine) could capture the physics benefits of both the SXD and XD. The hope is that it would inherit their capability to operate with Ar margin so that low core radiation can be sustained, at low separatrix density and good impurity segregation. The requirement to

have small impinging angles, but still above a certain threshold (1.5-2 degrees), implies that, to maximize flux expansion, the outer divertor leg must form a 90 degree angle with the divertor plate in the poloidal plane. In addition, its poloidal length should be shorter than the one we have analysed here, so that less extreme TF coil designs could be considered and the PF coils could remain closer to the plasma and improve control. In order to strengthen the coil cage, especially to out of plane deformations, we also suggest to implement box intercoil structures, as considered in the current I-DTT design. These consist of structures with larger effective poloidal cross section but hollow in the centre to keep them light.

Future work should develop the new configuration described above, but also include more refined multifluid and turbulent simulations, including kinetic neutral physics and an assessment of the poloidal variations of the diffusion coefficients. For a given configuration, further optimization of the divertor shape can also induce some benefits, as long as it complies with engineering constraints, which for DEMO are stringent. Also, neutronics studies will assess the amount of irradiation of the components as well as determine (comparatively) tritium breeding capabilities. Pumping studies have also been carried out and will be improved to ensure that fuel, ashes and impurities can be efficiently removed.

CRedit authorship contribution statement

F. Militello: Conceptualization, Methodology, Formal analysis, Resources, Writing, Visualization, Supervision, Project administration, Funding acquisition. **L. Aho-Mantila:** Supervision, Investigation, Formal analysis. **R. Ambrosino:** Methodology, Formal analysis, Resources, Supervision, Formal analysis, Investigation. **T. Body:** Formal analysis, Investigation. **H. Bufferand:** Resources, Formal analysis, Investigation. **G. Calabro:** Supervision. **G. Ciraolo:** Resources, Supervision. **D. Coster:** Methodology, Formal analysis, Supervision, Visualization. **G. Di Gironimo:** Formal analysis. **P. Fanelli:** Resources. **N. Fedorczak:** Resources. **A. Herrmann:** Resources. **P. Innocente:** Resources, Formal analysis, Investigation. **R. Kembleton:** Resources. **J. Lilburne:** Formal analysis, Visualization, Investigation. **T. Lunt:** Resources, Formal analysis, Software. **D. Marzullo:** Formal analysis, Visualization, Investigation. **S. Merriman:** Formal analysis, Visualization, Investigation. **D. Moulton:** Supervision, Formal analysis. **A.H. Nielsen:** Resources. **J. Omotani:** Resources, Software. **G. Ramogida:** Resources. **H. Reimerdes:** Resources. **M. Reinhart:** Resources, Funding acquisition. **P. Ricci:** Formal analysis. **F. Riva:** Resources, Formal analysis, Investigation. **A. Stegmeir:** Supervision, Formal analysis, Methodology, Software, Investigation. **F. Subba:** Formal analysis, Investigation. **W. Suttrop:** Resources. **P. Tamain:** Resources, Formal analysis, Investigation. **M. Teschke:** Resources. **A. Thysoe:** Resources. **W. Treutterer:** Resources. **S. Varoutis:** Formal analysis, Software, Investigation. **M. Wensing:** Formal analysis, Software, Investigation. **A. Wilde:** Supervision, Formal analysis. **M. Wischmeier:** Supervision, Resources. **L.Y. Xiang:** Formal analysis, Investigation.

Declaration of competing interest

The authors declare that they have no known competing financial interests or personal relationships that could have appeared to influence the work reported in this paper.

Acknowledgements

We acknowledge useful discussions with Prof. H. Zohm, Dr. G. Federici, Dr. C. Bachmann, Dr. F. Maviglia, Dr. M. Siccino, Dr. C. Vorpal, Dr. V. Corato and the WP-MAG team. This work has been carried out within the framework of the EUROfusion Consortium and has received funding from the Euratom research and training programme 2019–2020 under grant agreement No 633053. The views and opinions expressed herein do not necessarily reflect those of the European Commission. This work was partially funded by the RCUK Energy Programme [grant number EP/T012250/1]. To obtain further information on the data and models underlying this paper, whose release may be subject to commercial restrictions, please contact PublicationsManager@ccfe.ac.uk.

References

- [1] G. Federici, C. Bachmann, L. Barucca, C. Baylard, W. Biel, et al., *Nucl. Fusion* 59 (2019) 066013.
- [2] A. Loarte, B. Lipschultz, A.S. Kukushkin, et al., *Nucl. Fusion* 47 (2007) S203.
- [3] R.A. Pitts, X. Bonnin, F. Escourbiac, H. Frerichs, J.P. Gunn, et al., *Nucl. Mat. and Energy* 20 (2019) 100696.
- [4] H. Reimerdes, R. Ambrosino, P. Innocente, A. Castaldo, P. Chmielewski, et al., *Nucl. Fusion* 60 (2020) 066030.
- [5] D.D. Ryutov, *Phys. Plasmas* 14 (2007) 064502.
- [6] D.D. Ryutov, V.A. Soukhanovskii, *Phys. Plasmas* 22 (2015) 110901.
- [7] M. Kotschenreuther, P.M. Valanju, S.M. Mahajan, J.C. Wiley, *Phys. Plasmas* 14 (2007) 072502.
- [8] P.M. Valanju, M. Kotschenreuther, S.M. Mahajan, J. Canik, *Phys. Plasmas* 16 (2009) 056110.
- [9] L. Aho-Mantila, F. Subba, D.P. Coster, L. Xiang, F. Militello, T. Lunt, D. Moulton, H. Reimerdes, M. Wensing, M. Wischmeier, R. Ambrosino, X. Bonnin, M. Siccino, Predicted divertor asymmetries and their implications for choosing between a single and a double-null configuration for DEMO, in: 24th PSI Conference, Jeju, Korea, 2021.
- [10] E. Kaveeva, V. Rozhansky, I. Senichenkov, E. Sytova, I. Veselova, S. Voskoboinikov, X. Bonnin, R.A. Pitts, A.S. Kukushkin, S. Wiesen, D. Coster, *Nucl. Fusion* 60 (2020) 046019.
- [11] L.Y. Xiang, et al., Understanding the effects of super-X divertor on optimizing DEMO operation space, in: 24th PSI Conference, Jeju, Korea, 2021.
- [12] L. Xiang, F. Militello, D. Moulton, F. Subba, L. Aho-Mantila, D. Coster, M. Wensing, T. Lunt, M. Wischmeier, H. Reimerdes, Understanding the effects of super-X divertor configuration on optimizing operation space in DEMO, 2021, in preparation.
- [13] R. Moses, W.C. Young, Analytic expressions for magnetic forces on sectorized toroidal coils, in: 6th Symposium on Engineering Problems in Fusion Research, San Diego CA, 1975.
- [14] ITER report Magnet Structural Design Criteria Part 1: Main Structural Components and Welds, 2012.
- [15] O. Pan, T. Lunt, M. Wischmeier, D. Coster, The ASDEX Upgrade Team, *Plasma Phys. Control. Fusion* 60 (2018) 085005.
- [16] M. Giacomini, L.N. Stenger, P. Ricci, *Nucl. Fusion* 60 (2020) 024001.
- [17] D.D. Ryutov, R.H. Cohen, W.A. Farmer, T.D. Rognlien, M.V. Umansky, *Phys. Scr.* 89 (2014) 088002.
- [18] D. Galassi, P. Tamain, H. Bufferand, G. Ciraolo, Ph. Ghendrih, C. Baudoin, C. Colin, N. Fedorczak, N. Nace, E. Serre, *Nucl. Fusion* 57 (2017) 036029.
- [19] B. Lipschultz, F.L. Parra, I.H. Hutchinson, *Nucl. Fusion* 56 (2016) 056007.